Optica Applicata, Vol. XXXI, No. 2, 2001

Design considerations for GaAs/(AlGa)As SCH and GRIN-SCH quantum-well laser structures. I. The model

TOMASZ CZYSZANOWSKI, MICHAŁ WASIAK, WŁODZIMIERZ NAKWASKI*

Institute of Physics, Technical University of Łódź, ul. Wólczańska 219, 93–005 Łódź, Poland.

Some design modifications and optimization of the GaAs/(AlGa)As separate-confinement -heterostructure (SCH) as well as graded-index separate-confinement-heterostructure (GRIN -SCH) semiconductor lasers to reduce their room-temperature (RT) thresholds are discussed in the paper. To this end, a detailed optical model of arsenide diode lasers is developed and used to compare an impact of some structure details on RT lasing thresholds. In the model presented in this first part of the paper, both optical gain and losses are modeled rigorously. Optical fields within complex multi-layered structures of the SCH lasers are found using the downhill method. Threshold carrier concentrations are determined from the general balance of radiation gain and losses. As a result of the simulation, recommended basic design parameters for the above structures are deduced in the second part of the paper.

1. Introduction

As compared to classical double-heterostructure (DH) lasers (Fig. 1**a**), semiconductor lasers with single quantum well (SQW) active regions (Fig. 1**b**) exhibit much lower lasing thresholds, mostly because of the quantum-size effect [1], *i.e.*, lower quantized densities of states and higher carrier densities in two-dimensional (2D) QW structures. At the same time, however, efficiency η_{inj} of collecting injected carriers as well as optical confinement factor, Γ_{QW}, both in quantum-well (QW) active regions, are reduced, which prevents further improvement by application of arbitrarily thin QWs unless additional design features are added. The problem may be partly solved in multiple-quantum-well (MQW) lasers (Fig. 1**c**), in which both η_{inj} and Γ_{QW} are considerably improved. Another solution is possible in the separate-confinement-heterostructure lasers (Fig. 1**d**), where confinement mechanisms for carriers and an optical field may be optimized separately. Even better results are expected in graded-index separate-confinement-heterostructure

* Also with the Center for high Technology Materials, University of New Mexico, Albuquerque, NM 87131, USA.

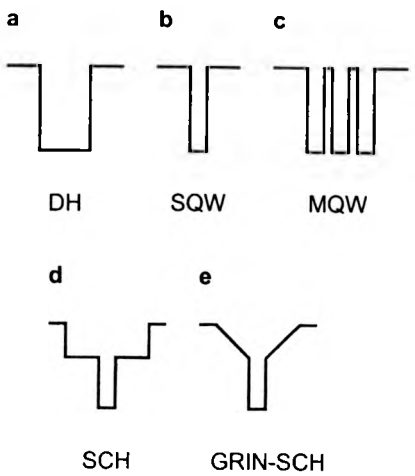

Fig. 1. Variations of the AlAs mole fraction in various structures of the GaAs/(AlGa)As lasers with: **a** – the double-heterostructure (DH) active region, **b** – the single-quantum-well (SQW) active region, **c** – the multiple-quantum-well (MQW) active region, **d** – the separate-confinement-heterostructure SQW (SCH-SQW) active region, and **e** – the graded-index SCH SQW (GRIN-SCH-SQW) active region.

(GRIN-SCH) shown in Fig. 1**e** (see, *e.g.*, [2], [3]) because of some additional phenomena, *i.e.*, the improved mode discrimination [4] and the built-in electric fields enhancing carrier capturing in QW active layers [5].

There are various possible designs of GRIN-SCH structures (see *e.g.*, Fig. 2), which may be very different from the standard one shown in Fig. 1**e**. Their efficiencies depend mostly on coupling between carriers and radiation field. On the other hand, profiles of optical fields in multilayered structures are very sensitive to construction details. Therefore the main goal of this work is to discuss an impact of some structure modifications of the GRIN-SCH-SQW lasers on their thresholds

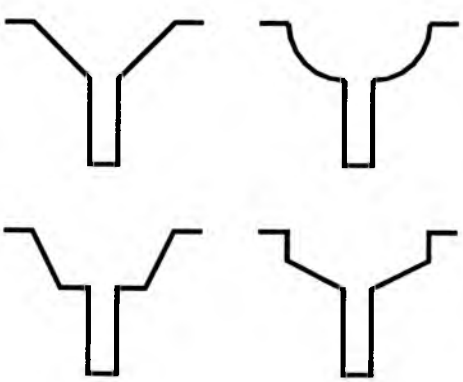

Fig. 2. Variation of the AlAs mole fraction in some possible designs of the GRIN-SCH-SQW active-layer structures.

using the comprehensive optical simulation of their operation. Also simpler SCH-SQW structures will be considered and compared to the above one. Some models of both the SCH lasers (see, *e.g.*, [6]) and the GRIN-SCH lasers (see *e.g.*, [3], [7], [8]) have already been reported. But, to the best of the author's knowledge, none of them have modeled the modified GRIN-SCH-SQW structures analyzed in this paper.

The article is organized as follows. The model used to simulate optical fields in laser structures is explained in this part of the paper, presenting in successive sections the complex wave equation and the algorithm of our computer calculations, the optical gain and loss determination, lasing threshold evaluation as well as optical field profiles within various SCH structures, which is followed by conclusions. The model will be used in the second part [9] of the paper to simulate operation of both the SCH-SQW lasers and the modified GRIN-SCH-SQW lasers.

2. Optical fields

Let us consider the sinusoidal time-varying optical field (see Fig. 3) of the m-th radiation mode travelling in the $0z$ direction within the j-th layer of the multilayer structure [$j \in (1, J)$] of a semiconductor laser and oscillating in the $0y$ direction (TE – transverse electric polarization)

$$E_{j,m}(x,y,t) = \vec{1}_y E_{j,m}(x) \exp[i(\omega_m t - \beta_m z)]. \tag{1}$$

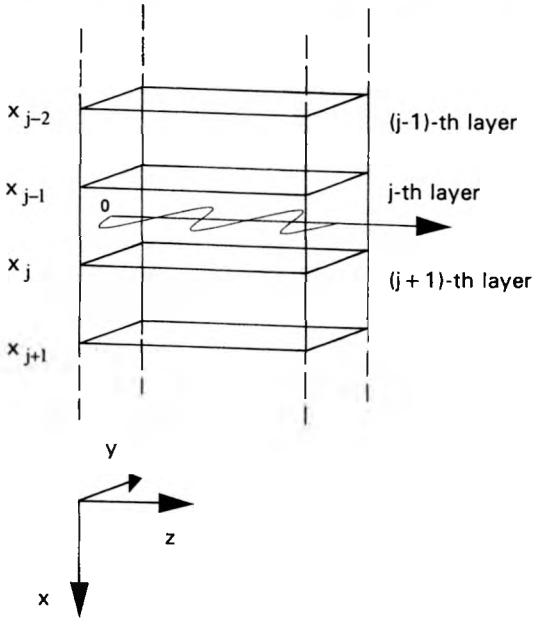

Fig. 3. Coordinate system and the layer notation used in our calculations.

In the above relation, $\vec{1}_y$ is the unit vector along the $0y$ direction, $E_{j,m}$ is the wave amplitude of the m-th radiation mode within the j-th structure layer, ω_m is the m-th mode angular frequency and β_m is the m-th mode propagation constant which in a lossy (gain) medium becomes a complex quantity

$$\beta_m = \beta_{m,r} + i\beta_{m,i}. \tag{2}$$

The complex mode amplitudes $E_{j,m}$ are solutions of the complex wave equation [10]

$$\frac{d^2 E_{j,m}(x)}{dx^2} - (\beta_m^2 - k_m^2 N_{R,j}^2) E_{j,m}(x) = 0 \tag{3}$$

where k_m is the free-space wave number ($k_m = 2\pi/\lambda_m$ with λ_m being the wavelength) and $N_{R,j}$ is the complex index of refraction of the j-th layer material

$$N_{R,j} = n_{R,j} - ik_{e,j}. \tag{4}$$

With an exception of graded-index layers, all structure layers are assumed to be uniform, *i.e.*, they are characterized by indices of refraction $n_{R,j}$ and extinction coefficients $k_{e,j}$ which are constant within each of them. Within the GRIN layers, on the other hand, values of both the above coefficients are directly associated with a local AlAs mole fraction. In the numerical calculations, these graded layers are divided into 20 equal uniform parts. An increase in their number does not improve the exactness of the method.

A general solution of wave equation (3) may be expressed in the form of a superposition of two waves running in the opposite ($+0x$ and $-0x$) directions

$$E_{j,m}(x) = A_{j,m} \exp[+y_{j,m}(x - x_j)] + \beta_{j,m} \exp[-y_{j,m}(x - x_j)] \tag{5}$$

where x_j is the coordinate of the boundary between the j-th and the $(j+1)$-th layers (*cf.*, Fig. 3), and

$$\gamma_{j,m}^2 \equiv \beta_m^2 - k_m^2 N_{R,j}^2. \tag{6}$$

The complex coefficients $A_{j,m}$ and $\beta_{j,m}$ are to be determined from the boundary conditions using the following recursive matrix approach proposed by BERGMANN and CASEY [11]. As usual, for each m-th mode, both the electric field and its derivative in the $0x$ direction are assumed to be continuous at each structure interface:

$$A_{j,m} \exp(+\gamma_{j,m} d_j) + B_{j,m} \exp(-\gamma_{j,m} d_j) = A_{j+1,m} + B_{j+1,m}, \tag{7}$$

$$\gamma_{j,m}[A_{j,m} \exp(+\gamma_{j,m} d_j) - B_{j,m} \exp(-\gamma_{j,m} d_j)] = \gamma_{j+1,m}(A_{j+1,m} - B_{j+1,m}) \tag{8}$$

where $d_j = x_j - x_{j-1}$ is the thickness of the j-th layer. Using the following matrix form:

$$T_{j,m} = \begin{bmatrix} a_{j,m}^+ e_{j,m}^+ & a_{j,m}^- e_{j,m}^- \\ a_{j,m}^- e_{j,m}^+ & a_{j,m}^+ e_{j,m}^- \end{bmatrix} \tag{9}$$

with:

$$a_{j,m}^{\pm} \equiv 1 \pm \frac{\gamma_{j,m}}{\gamma_{j+1,m}}, \tag{10}$$

$$e_{j,m}^{\pm} \equiv \frac{1}{2} \exp(\pm \gamma_{j,m} d_j), \tag{11}$$

the coefficients for adjacent layers may be connected with each other

$$\begin{bmatrix} A_{j+1,m} \\ B_{j+1,m} \end{bmatrix} = T_{j,m} \begin{bmatrix} A_{j,m} \\ B_{j,m} \end{bmatrix}. \tag{12}$$

For guided modes, amplitudes should decay at infinity, which means that $B_{1,m} = A_{J,m} = 0$, which which is followed by

$$\begin{bmatrix} 0 \\ B_{J,m} \end{bmatrix} = T_{J,m}^{*} \begin{bmatrix} A_{1,m} \\ 0 \end{bmatrix} \tag{13}$$

with

$$T_{J,m}^{*} \equiv \prod_{j=1}^{J} T_{j,m} \equiv \begin{bmatrix} t_{11} & t_{12} \\ t_{21} & t_{22} \end{bmatrix}. \tag{14}$$

For Equation (13) to be fulfilled

$$t_{11}(\beta_m) = 0, \tag{15}$$

which is used to determine (see below) the mode complex propagation constants β_m and enables us to determine the optical field of all m-th modes in all j-th structure layers using Eq. (5) and the $A_{j,m}$ and $B_{j,m}$ coefficients found with the aid of recursive relation (12). Additionally, we may find for each m-th mode its effective index of refraction $n_{\mathrm{eff},m}$ and effective loss coefficient $\alpha_{\mathrm{eff},m}$ directly from both parts, real and imaginary, of the m-th mode propagation constant:

$$n_{\mathrm{eff},m} = \frac{\beta_{m,r}}{k_m}, \tag{16}$$

$$\alpha_{\mathrm{eff},m} = 2\beta_{m,i}. \tag{17}$$

To find roots $\beta_m = \beta_{m,r} + i\beta_{m,i}$ of Eq. (15), successive minima of $F(\beta) = |t_{11}(\beta)|^2$ are determined using the "downhill method" developed by SCHLERETH and TACKE [12]. The minima are sought within the area $n_{R,\max} \geqslant \beta_{m,r} \geqslant 0.8 n_{R,\max}$ and $-0.01 \leqslant \beta_{m,i} \leqslant 0.01$, where $n_{R,\max}$ is the maximal value of an index of refraction inside the waveguide. From all β_m values corresponding to all minima of $F(\beta)$, the starting complex β_0 guess value is chosen as that with the biggest real part. Then F is determined for four surrounding points corresponding to $\beta_0 \pm i\Delta$ and $\beta_0 \pm \Delta$,

where $\Delta = bF(\beta_0)$. The one for which F achieves the smallest value is chosen as the next guess point and the stepwidth Δ is increased by 10%. If there are two or more smallest values or $F(\beta_0)$ is a minimum, the stepwidth is reduced to $\Delta/2$. The algorithm is terminated when $\Delta < \varepsilon$, where ε is the assumed accuracy. In the calculation, $b = 10^{-6}$ and $\varepsilon = 10^{-16}$ were found to be reasonable choices.

From now on, we will omit the subscripts m, because we will consider only one (fundamental) radiation mode.

3. Optical gain

Using the Fermi Golden Rule [13] and the envelope/Bloch function formalism for the electron and hole wave functions, the probability W (per unit time) of the stimulated band-to-band transitions in 2D semiconductor structures may be expressed in the following form [14]:

$$W = \frac{2\pi e^2 |A_0|}{m_0^2 \hbar} |M_T|^2 \rho_r(\hbar\omega) \tag{18}$$

where e is the unit charge, m_0 is the electron rest mass, $\hbar = h/2\pi$, A_0 is the amplitude of the vector potential of the plane wave considered, ω is its angular frequency, M_T is the transition matrix element [15] and ρ_r stands for the reduced density of states. Then the optical gain g_n for the n-th pair of energy levels (one level in the conduction band and the second one in the valence band) may be written as

$$g_n(\hbar\omega) = \frac{e^2\pi}{n_R c m_0^2 \varepsilon_0 \omega} |M_T|^2 \rho_r(\hbar\omega)[f_c(E_c) - f_v(E_v)] \tag{19}$$

where n_R is the refractive index, c stands for the speed of light in vacuum, ε_0 is the dielectric constant of the vacuum, f_c and f_v – the quasi-Fermi functions for the conduction band and the valence band, respectively, and $E_c - E_v = \hbar\omega$.

To determine the total optical gain spectrum, $g_T(\omega)$, all possible band-to-band transitions between energy levels in the conduction band and both the light-hole *lh* and heavy-hole *hh* valence bands should be taken into account

$$g_T(\hbar\omega) = \sum_{lh} g_{lh}(\hbar\omega) + \sum_{hh} g_{hh}(\hbar\omega) \tag{20}$$

where the first sum comprises pairs of states in the conduction band and the light-hole valence band separated by the energy $\hbar\omega$, whereas the second sum contains analogous pairs of states in the conduction band and the heavy-hole valence band.

In the calculations, the following polarization-dependent matrix element is used for 2D structures [15], [16]:

$$|M_T|^2 = \begin{cases} |M|^2(1-e_x^2) & \text{for heavy holes} \\ |M|^2(1/3+e_x^2) & \text{for light holes} \end{cases} \tag{21}$$

where $|M|^2 = (14.4 \pm 0.8)\,\mathrm{eV}\cdot m_0$ [17] and e is the unit vector along the radiation vector potential A. Its x-component, e_x, is assumed to be directed parallely to the electron k-vector (*i.e*,. along the $0x$ axis). Therefore for the TE modes: $e_y^2 = 1$ (or $e_x^2 = 0$), whereas for the TM (transverse magnetic) modes: $e_y^2 = 0$ (or $e_x^2 = 1$).

Additionally, the effect of line-shape broadening of both transition energy levels (because of the intraband relaxation processes such as the carrier-carrier scattering and the carrier-phonon scattering [18]) is included. To this end, the original approach [19] has been used with the aid of integration over all transition energies weighted for both the upper and the bottom energy levels by the Lorentzian line-shape functions [20], [21].

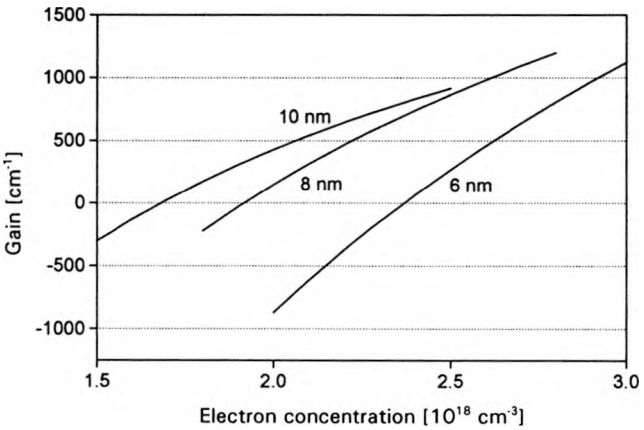

Fig. 4. Calculated profiles of the maximal optical gain at room temperature versus electron concentrations within the GaAs/$Al_{0.3}Ga_{0.7}As$ SQW active layers of various widths d_{QW}.

Example results of our gain calculations for typical GaAs/$Al_{0.3}Ga_{0.7}As$ SQWs are shown in Fig. 4. Successive curves present plots of a maximal optical gain calculated for the above 6-nm (60-Å), 8-nm (80-Å) and 10-nm (100-Å) SQW active layers, respectively, versus electron concentration n. Their intersections with the gain = 0 axis indicate the transparency concentrations, whereas their slopes correspond to the differential gains ($\partial g/\partial n$), being, as one can see, slowly reduced with an increase in n.

4. Optical losses and refractive indices

There are two kinds of absorption taken into account in our model: the band-to-band absorption (within all semiconductor layers except the active layers) and the free-carrier absorption (all semiconductor layers). On the basis of the experimental results reported by ADACHI [22], we have found the following relation for the band-to-band absorption coefficient (in cm^{-1}) in the $Al_xGa_{1-x}As$ for $\lambda > 815$ nm

$$\alpha_{bb}(x,\lambda) = \exp\left[(a_1 + b_1 x + c_1 x^2) + (a_2 + b_2 x + c_2 x^2)\lambda\right] \tag{22}$$

where for the room temperature: $a_1 = 31.430$, $b_1 = 7.2385$, $c_1 = 287.39$, $a_2 = -3.0243 \cdot 10^5$ cm^{-1}, $b_2 = 1.3327 \cdot 10^4$ cm^{-1}, and $c_2 = -6.1500 \cdot 10^6$ cm^{-1}. Analogous RT free-carrier absorption coefficients (in cm^{-1}) are found from the relations given by Weber [23]

$$\alpha_{fc}(n,p) = 3.13 \cdot 10^{-18} n + \exp\left[2.856 (10^{-18} p)^{0.1723}\right] \tag{23}$$

where the carrier concentrations n and p should be given in cm^{-3}.

In the optical model, diffraction losses, *i.e.*, unfavourable penetration of passive areas by the optical field, are introduced by the method itself. No possible absorption processes other than the ones described above nor scattering losses are included; they may, however, be considerably reduced using a sophisticted technology. Also end losses, being a result of emission of an output beam, are omitted. The last loss mechanism is, however, practically the same for all TE radiation modes, therefore it may be considered only as an additional factor increasing proportionally all lasing thresholds.

At temperatures close to RT, the index of refraction in the $Al_xGa_{1-x}As$ material may be expressed as follows [24]:

$$n_R(x,T,n,p) = (3.590 - 0.710x + 0.091x^2)\left[1 + (T - 297\ \text{K})\, 4.9 \cdot 10^{-4}\,\text{K}^{-1}\right] - 1.2 \cdot 10^{-20}\ \text{cm}^{-3}(n+p). \tag{24}$$

5. Lasing threshold

The lasing threshold may be found from the following balance of radiation gain and losses:

$$\Gamma_{QW} g_{th} = \sum \text{losses} \tag{25}$$

where Γ_{QW} is the confinement factor of the radiation field in the QW active region and g_{th} is the threshold gain. Both the optical gain and the free-carrier absorption in the active region depend on the carrier concentrations $n = p$ within it. Therefore, the balance equation (25) is fulfilled for the specified threshold carrier concentration n-th, which is directly associated with the threshold current density j-th

$$j_{th} = A n_{th} + B n_{th}^2 + C n_{th}^3 + j_l(n_{th}) \tag{26}$$

where A, B, and C are the proportional coefficients and j_l is the leakage current density.

The imaginary part of the complex propagation constant is directly connected with the effective radiation losses or gain (*cf.* Eq. (17)). Therefore the threshold value of the active-region carrier concentration n-th is found in this approach from the condition that the propagation constant becomes real (*cf.* Eq. (2))

$$\beta_i (n = n_{th}) = 0. \tag{27}$$

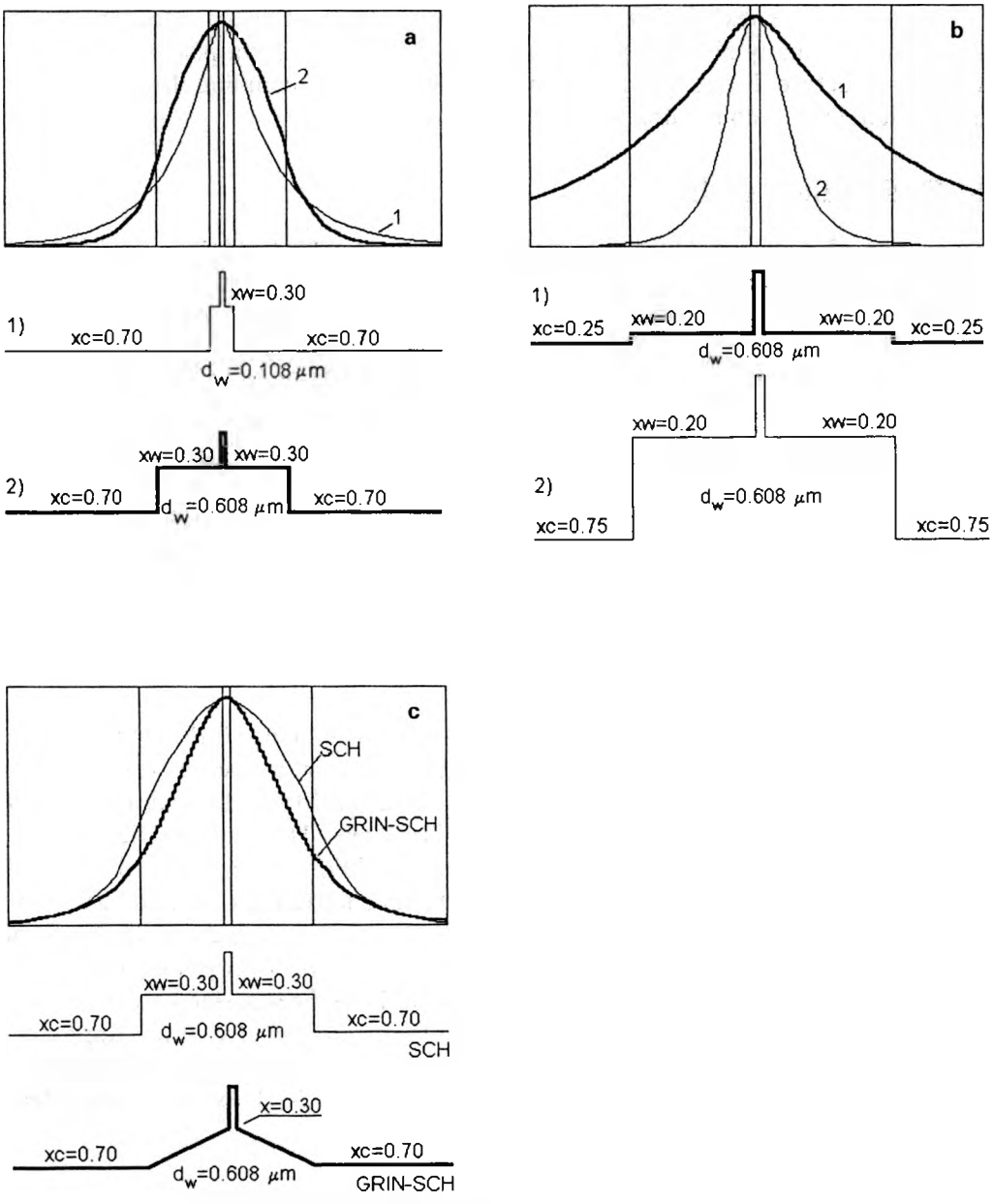

Fig. 5. Comparison between relative optical intensity profiles within various SQW ($d_{QQ} = 8$ nm) GaAs/(AlGa)As SCH structures with: **a** — the 0.108-μm or 0.608-μm $Al_{0.3}Ga_{0.7}As$ waveguide and $Al_{0.7}Ga_{0.3}As$ claddings, **b** — the 0.608-μm $Al_{0.2}Ga_{0.8}As$ waveguide and $Al_{0.25}Ga_{0.75}As$ or $Al_{0.75}Ga_{0.25}As$ claddings, and **c** — the 0.608-μm $Al_{0.3}Ga_{0.7}As$ waveguide or GRIN (AlGa)As waveguide with an linear change of the AlAs mole fraction from 0.7 to 0.3 and the $Al_{0.7}Ga_{0.3}As$ claddings. For all the structures under consideration, profiles of an index of refraction are shown schematically. All optical profiles are normalized to the same amplitude within the SQW GaAs active layer.

It should be stressed that the above simple condition takes into account in a natural way many physical phenomena, including nonuniform penetration of the various structure layers by the radiation field, its outcoupling losses and its interaction with recombining carriers in active regions.

6. Optical-field profiles

Some typical optical-field profiles determined for the GaAs/(AlGa)As SCH and GRIN-SCH structures using the approach explained in Section 2 are shown in Fig. 5. In particular, Fig. 5**a** shows an impact of the $Al_{0.3}Ga_{0.7}As$ waveguide width d_W (0.108 μm or 0.608 μm). As one can see, the narrowing of the waveguide is followed by an unprofitable leakage of the field. Analogously, Fig. 5**b** illustrates an impact of the refractive index step at the waveguide/cladding interface on a confinement of the field. Figure 5**c**, in turn, enables comparison between the SCH and the GRIN-SCH structures. Seemingly, the graded profile of the GRIN-SCH structure confines better the optical field, but in fact the SCH profile is over that of the GRIN-SCH one not only beyond the waveguide but also within it. Therefore it needs some detailed calculations to determine which of the waveguides works better.

7. Conclusions

A detailed optical model of multi-layered structures of GaAs/(AlGa)As separate -confinement-heterostructure lasers, *i.e.*, simple SCH lasers as well as graded-index SCH lasers, is presented. The "downhill method" is used to find profiles of optical fields within the complex structures of the SCH lasers. Threshold carrier concentrations are determined from a general threshold condition expressing the balance of radiation gain and losses. In the model, optical gain spectra are calculated using the original approach including broadening of both transition levels. Two kinds of absorption are taken into account: the band-to-band absorption (within all semiconductor layers except the active layers) and the free-carrier absorption (all semiconductor layers). Additionally, diffraction losses are included in this approach.

The model has been developed to be used in the second part [9] of the paper to discuss usability of possible structure modifications of the SCH lasers to reduce their room-temperature thresholds.

Acknowledgments — This work was supported by the Polish State Committee for Scientific Research (KBN), grant Nos. 8-T11B-018-12, 7-T11-073-21, 7-T11B-045-21, and by the US–Poland Maria Skłodowska-Curie Joint Fund No. MEN/NSF-98-336.

References

[1] COLDREN L. A., CORZINE S. W., *Diode Lasers and Photonic Integrated Circuits*, J. Wiley & Sons, Inc., New York, 1995, Chapters 4.3 and 4.6.

[2] BUGAJSKI M., KANIEWSKA M., REGIŃSKI K., *et al.*, Electron. Technol. **29** (1996), 346.

[3] BUGAJSKI M., KANIEWSKA M., REGIŃSKI K., *et al.*, Proc. SPIE **3186** (1997), 310.
[4] TSANG W.T., Appl. Phys. Lett. **39** (1981), 134.
[5] HERSEE S., BALDY M., ASSENAT P., *et al.*, Electron. Lett. **18** (1982), 618.
[6] WENZEL H., WÜNSCHE H.-J, Phys. Stat. Sol. A **120** (1990), 661.
[7] CHINN S.R., ZORY P.S., REISINGER A.R., IEEE J. Quantum Electron. **24** (1988), 2191.
[8] LI Z.-M., DZURKO K.M., DELAGE A., MCALISTER S.P., IEEE J. Quantum Electron. **28** (1992), 792.
[9] CZYSZANOWSKI T., WASIAK M., NAKWASKI W., Opt. Appl. **31** (2001), 325.
[10] MROZIEWICZ B., BUGAJSKI M., NAKWASKI W., *Physics of Semiconductor Lasers*, North Holland, Amsterdam, 1991, Chapter 4.1.
[11] BERGMANN M.J., CASEY H.C., Jr., J. Appl. Phys. **84** (1998), 1196.
[12] SCHLERETH H.-K., TACKE M., IEEE J. Quantum Electron. **26** (1990), 627.
[13] Ref. 1, Appendix 9.
[14] WASIAK M., *Optical gain in the laser with a quantum active region* (in Polish), MSc dissertation, Technical University of Łódź, Faculty of Technical Physics, Computer Science and Applied Mathematics, 1999.
[15] Ref. 1, Appendix 10.
[16] ZORY P.S., Jr., [Ed.] *Quantum Well Lasers*, Academic Press, Boston, 1993.
[17] HERMANN C., WEISBUCH C., Phys. Rev. B **15** (1977), 823.
[18] ASADA M., IEEE J. Quantum Electron. **25** (1989), 2019.
[19] WASIAK M., BUGAJSKI M., submitted to Electron Technology.
[20] Ref. 1, Chapter 4.3.2.
[21] ELISEEV P.G., Electron. Lett. **33** (1997), 2046.
[22] ADACHI S., *GaAs and Related Materials. Bulk Semiconducting and Superlattice Properties*, World Scientific, Singapore, 1994, Fig. 11.50, p. 387.
[23] WEBER J.-P., *Propagation of light in periodic structures: Application to the surface-emitting laser-diode*, PhD dissertation, University of California at Berkeley, 1990, Appendix A, pp. 234–236.
[24] NAKWASKI W., Opt. Appl. **29** (1989), 313.

Received October 9, 2000